



TECHNICAL NOTE



Explaining long-range fluid pressure transients caused by oilfield wastewater disposal using the hydrogeologic principle of superposition

Ryan M. Pollyea¹

Received: 10 April 2019 / Accepted: 18 October 2019 / Published online: 27 November 2019
© Springer-Verlag GmbH Germany, part of Springer Nature 2019

Abstract

Injection-induced earthquakes are now a regular occurrence across the midcontinent United States. This phenomenon is primarily caused by oilfield wastewater disposal into deep geologic formations, which induces fluid pressure transients that decrease effective stress and trigger earthquakes on critically stressed faults. It is now generally accepted that the cumulative effects of multiple injection wells may result in fluid pressure transients migrating 20–40 km from well clusters. However, one recent study found that oilfield wastewater volume and earthquake occurrence are spatially cross-correlated at length-scales exceeding 100 km across Oklahoma. Moreover, researchers recently reported observations of increasing fluid pressure in wells located ~90 km north of the regionally expansive oilfield wastewater disposal operations at the Oklahoma-Kansas border. Thus, injection-induced fluid pressure transients may travel much longer distances than previously considered possible. This study utilizes numerical simulation to demonstrate how the hydrogeologic principle of superposition reasonably explains the occurrence of long-range pressure transients during oilfield wastewater disposal. The principle of superposition states that the cumulative effects of multiple pumping wells are additive and results from this study show that just nine high-rate injection wells drives a 10-kPa pressure front to radial distances exceeding 70 km after 10 years, regardless of basement permeability. These results yield compelling evidence that superposition is a plausible mechanistic process to explain long-range pressure accumulation and earthquake-triggering in Oklahoma and Kansas.

Keywords Salt water disposal · Wastewater · Earthquake · Injection wells · Numerical modeling

Introduction

The central and eastern United States (CEUS) averaged ~19 magnitude-3 or greater (M3+) earthquakes per year before 2009 (Fig. 1, blue circles), but this average rate exceeded 400 per year between 2009 and 2018 (Fig. 1, red circles). This 20-fold increase in the M3+ earthquake rate is caused by oilfield wastewater disposal in deep injection wells, which induces fluid pressure transients that trigger earthquakes

(Keranen et al. 2014; Keranen et al. 2013; Ellsworth 2013). Injection-induced earthquakes have been reported in Wyoming, Colorado, New Mexico, Texas, Ohio, Kansas, and Arkansas (NRC 2013; Weingarten et al. 2015), but they are most pronounced in Oklahoma, where the rate of M3+ earthquakes increased from ~1 year⁻¹ before 2009 to over 2.5 day⁻¹ in 2015 (Pollyea et al. 2018a). The rapid onset of seismicity in Oklahoma led to a number of regulatory changes, which, in combination with declining prices in the oil and gas markets, have been attributed to declining earthquake frequency since 2015. Nevertheless, Oklahoma experienced three M5+ earthquakes in 2016 and there were 412 M3+ earthquakes across the CEUS in 2018.

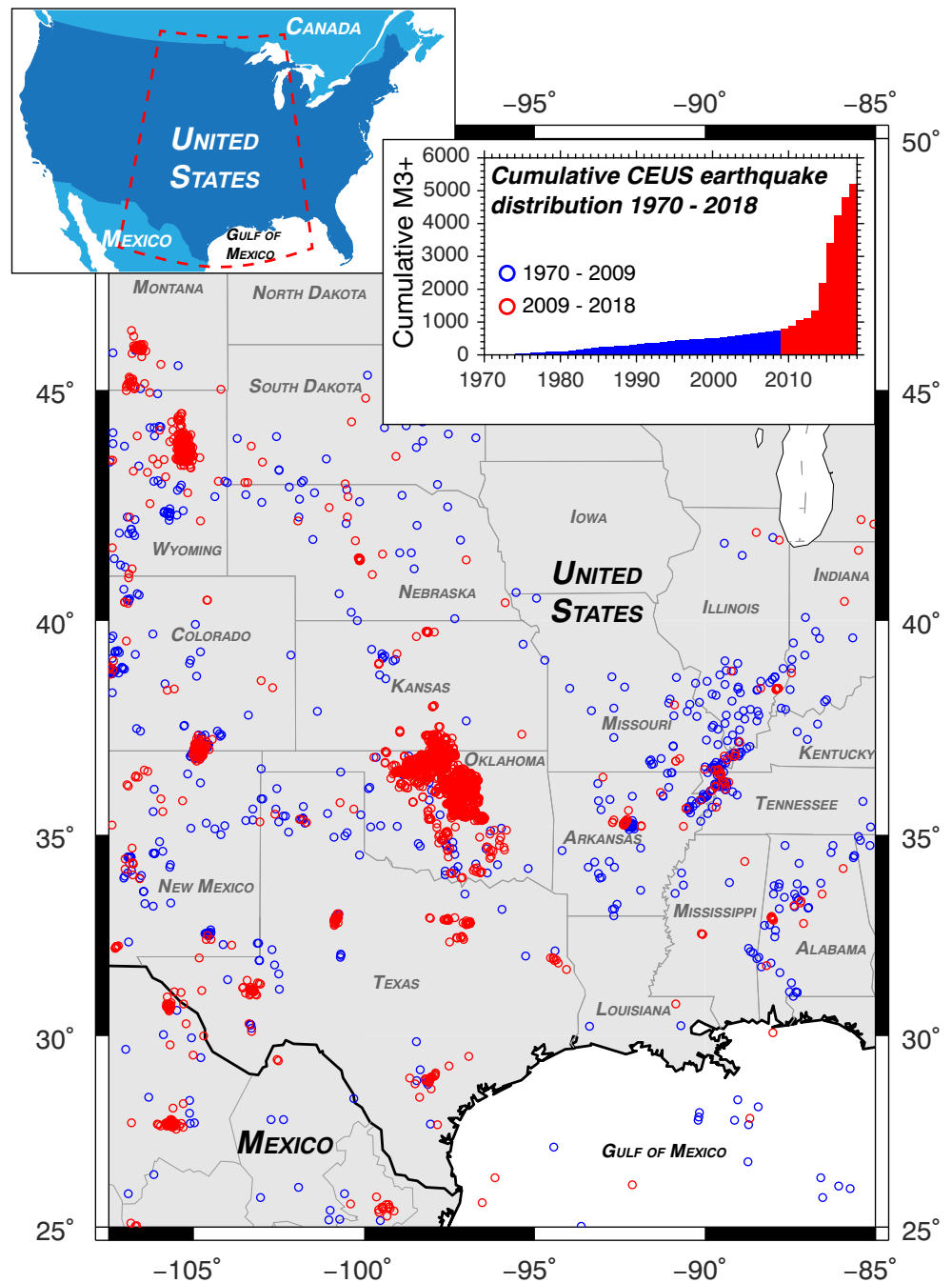
Injection-induced earthquakes are reasonably explained by the application of effective stress theory to the Mohr-Coulomb failure criterion (NRC 2013). Specifically, the effective normal stresses acting on a fault decreases in equal proportion to a rise in fluid pressure less any poro-elastic relaxation (Zoback and Hickman 1982). Given a sufficient

Electronic supplementary material The online version of this article (<https://doi.org/10.1007/s10040-019-02067-z>) contains supplementary material, which is available to authorized users.

✉ Ryan M. Pollyea
rpollyea@vt.edu

¹ Department of Geosciences, Virginia Polytechnic Institute and State University, Blacksburg, VA, USA

Fig. 1 Spatial and temporal (right inset) distribution M3+ earthquakes in the central and eastern United States from January 1, 1970 to December 31, 2018. Data from USGS ComCat database (USGS 2019). Figure design adapted from Fig. 2 in Ellsworth (2013). Upper left inset shows the regional extent of the central and eastern United States (dashed red line)



rise in pore fluid pressure within faults optimally aligned to the regional stress field, the effective normal stress may drop below the Mohr-Coulomb failure threshold triggering the release of previously accumulated strain energy into the surrounding rock (Raleigh et al. 1976; Hubbert and Willis 1957). The seismic moment of injection-induced earthquakes is governed by fault shear modulus, rupture area, and displacement, while their occurrence is largely controlled by interactions between injection-induced fluid pressure transients and faults optimally aligned with the regional stress field (Walsh and Zoback 2015; Shapiro et al. 2011).

The linkage between oilfield wastewater disposal, fluid pressure transients, and earthquake occurrence in Oklahoma, USA, was originally reported by Keranen et al. (2014). This landmark study showed that high-rate wastewater injection wells near Oklahoma City caused a pressure front to migrate over 40 km from the well cluster and the temporal progression of this pressure front accurately matched the 2011 Jones earthquake swarm. Similarly, Goebel et al. (2017) showed that the 2016 M5.1 earthquake sequence in Fairview, Oklahoma likely resulted from wastewater injection wells located ~40 km away, although this study, as well as Goebel and

Brodsky (2018), suggests that poro-elastic stress transfer may also trigger earthquakes at long radial distances from injection wells. Nevertheless, history-matching groundwater models are now widely implemented to link oilfield wastewater disposal with earthquake swarms, e.g., in Milan, Kansas (Hearn et al. 2018), Greeley, Colorado (Brown et al. 2017), Dallas-Fort Worth, Texas (Ogwari et al. 2018), and Guthrie, Oklahoma (Schoenball et al. 2018). These studies show that oilfield wastewater disposal causes pressure transients (≥ 10 kPa) that induce earthquakes at lateral distances of 20–40 km away from injection wells.

At the regional-scale, several recent studies focusing on central Oklahoma and southern Kansas show that injection-induced pressure transients may travel much farther distances than previously considered possible. For example, Langenbruch et al. (2018) developed a regional-scale model of oilfield wastewater disposal that shows injection-induced pressure transients may extend 50+ km north of the well fields located near the border separating Oklahoma and Kansas. Similarly, Pollyea et al. (2018a) presented a geostatistical analysis showing that earthquake occurrence and wastewater disposal volume are spatially cross-correlated at length-scales exceeding 100 km. This latter study was disputed in the media because the geostatistical correlations do not explain the *process* responsible for this long-range phenomenon (Wilmoth 2018); however, Peterie et al. (2018) later reported *observations* of increasing fluid pressure in deep monitoring wells, as well as earthquake swarms as far away as 90 km from high-rate injection wells at the Kansas-Oklahoma border (Peterie et al. 2018). In an explicit acknowledgement of the difficulty explaining long-range pressure accumulation, Peterie et al. (2018) state, “...pressure diffusion from cumulative disposal to the south likely induced earthquakes much farther than previously documented from individual injection wells.” While the scientific community generally agrees that “cumulative disposal” from numerous high-rate wastewater injection wells is driving pressure transients over extraordinary lateral distances, the *mechanistic process* responsible for these cumulative effects has not been clearly documented in the literature. As a consequence, statistical analyses of long-range earthquake triggering (Pollyea et al. 2018a) are met with skepticism (Wilmoth 2018) and observations of long-range fluid pressure accumulation do not have a defensible mechanistic explanation (Peterie et al. 2018).

This study implements high-fidelity, multi-physics numerical simulation to show that the hydrogeological principle of superposition reasonably explains recent reports of long-range pressure transients caused by oilfield wastewater disposal. As a mechanistic process, the principle of superposition simply states that pressure transients from closely spaced injection wells will merge to locally increase the hydraulic gradient, thus driving fluid pressure much longer distances than is possible from wells operating in isolation.

Methods

To understand the hydrogeology of long-range pressure transients during oilfield wastewater disposal, this study models several hypothetical wastewater injection scenarios using characteristics of the Anadarko Shelf geologic province of north-central Oklahoma. Between 2011 and 2015, this region experienced rapid increases in both oilfield wastewater disposal and earthquake occurrence (Pollyea et al. 2018b, 2019). The primary target reservoir for oilfield wastewater disposal is the Arbuckle formation, which is in direct hydraulic communication with the underlying Precambrian basement (Johnson 1991). The geologic model reproduces the Arbuckle formation from 1,900 to 2,300-m depth overlying the Precambrian basement from 2,300 to 10,000 m depth. The model domain comprises a 200 km \times 200 km lateral extent; however, four-fold symmetry is invoked to reduce the simulation grid to a lateral extent of 100 km in each direction. As a result, the 100 km \times 100 km \times 8.1 km volume is modeled as a three-dimensional (3D) unstructured grid comprising 1,278,613 grid cells with local grid refinement near the injection wells (Fig. 2a). The Arbuckle formation is modeled as an isotropic and homogeneous porous medium with permeability of 5×10^{-13} m² (Fig. 2b). The Precambrian basement is discretized as a dual continuum (2 vol.% fracture domain) to separately account for fracture and matrix flow. Basement fracture permeability (k) decays with depth (z) in accordance with the Manning and Ingebritsen (1999) equation: $k(z) = k_0 (z/z_0)^{-3.2}$. For this model, z_0 corresponds with the depth of the Arbuckle-basement contact (2,300 m), where fracture permeability is estimated to be 1×10^{-13} m². As a result, the volume-weighted effective (bulk) permeability ranges from 2×10^{-15} m² at the Arbuckle-basement interface to 2×10^{-17} m² at 10 km depth (Fig. 2b). These effective permeability values are congruent with basement permeability values reported in the literature for northern and central Oklahoma (Keranen et al. 2014; Goebel et al. 2017). Because permeability within the Precambrian basement is highly uncertain, three additional permeability scenarios are tested for $k(z_0)$ equal to 5×10^{-13} m², 5×10^{-14} m², and 1×10^{-14} m² (Fig. S1 of the electronic supplementary material ESM). The remaining hydraulic and thermal parameters are listed in Table 1.

To compare pressure accumulation between a single isolated injection well and multiple closely spaced injection wells, this study considers two oilfield wastewater disposal scenarios: (1) an individual well operating within the upper 200 m of the Arbuckle formation at 2,080 m³ day⁻¹ (13,000 US barrels (bbl) day⁻¹), and (2) a well field comprising nine injection wells with 6 km spacing, each operating at 2,080 m³ day⁻¹ (13,000 bbl day⁻¹). All model scenarios simulate 10 years of oilfield wastewater disposal followed by 10 years of post-injection fluid pressure recovery. These models also account for variable fluid composition, which has been shown to drive

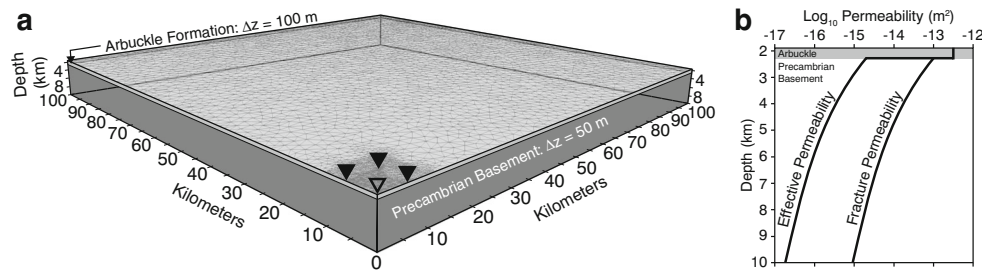


Fig. 2 Schematic illustration of the **a** model domain and **b** permeability structure. The conceptual geologic model represents the Arbuckle formation from 1,900 to 2,300-m depth and Precambrian basement from 2,300 to 10,000-m depth. The model is discretized as an unstructured grid comprising 1,278,613 grid cells with grid refinement near the injection wells (inverted triangles). For the single-well model

fluid pressure transients deeper into the seismogenic zone even after injection operations cease (Pollyea et al. 2019). The wastewater is representative of brine produced from the Mississippi Lime formation, which is reported to have a mean total dissolved solids (TDS) concentration of 207,000 ppm (Blondes et al. 2017). This TDS concentration corresponds with a fluid density of $1,123 \text{ kg m}^{-3}$ at conditions (21 MPa and 40°C) representative of the disposal reservoir (Mao and Duan 2008). Fluid composition within the Precambrian basement is based on data from south-central Kansas, which indicate that the mean TDS concentration is 107,000 ppm (Blondes et al. 2017) with corresponding fluid density of $1,068 \text{ kg m}^{-3}$ at 21 MPa and 40°C (Mao and Duan 2008).

The initial temperature distribution is calculated on the basis of a 40 mW m^{-2} heat flux reported for Oklahoma (Cranganu et al. 1998). This heat flux results in a geothermal gradient of 18°C km^{-1} . Initial fluid pressure is 21 MPa in the Arbuckle formation and increases as the product of depth, gravitational acceleration, and fluid density, the latter of which is dependent on the thermal gradient. Dirichlet conditions are specified in the far field to maintain the initial pressure and temperature gradients along the lateral boundaries. Adiabatic pressure boundaries are specified across the top and bottom of the domain on the basis of low permeability shale overlying the Arbuckle formation and exceedingly low permeability at $\sim 10 \text{ km}$ depth. The basal boundary also imposes the 40 mW m^{-2} regional heat flux as a Neumann condition. Adiabatic boundaries are also specified in the xz - and

only the central well is operating (open triangle). The Precambrian basement is modeled as a dual continuum with 98 vol% matrix and 2 vol% fracture. **b** Presents the fracture permeability and volume-weighted effective permeability. Note that the model domain invokes four-fold symmetry, so the one-quarter domain accounts for the effects of nine injection wells when all wells are operating

yz -planes through the origin to facilitate the symmetry boundaries.

The code selection for this study is TOUGH3 (Jung et al. 2017) compiled with equation of state module EOS7 for simulating non-isothermal mixtures of pure water and brine with mixing by advective transport and molecular diffusion. The TOUGH3 simulator solves the governing equations for mass and heat flow with parallel numerical solvers (PetSc), which allows for extremely high-resolution numerical simulation. The complete solution scheme for TOUGH3 is presented in the TOUGH3 User's Guide (Jung et al. 2018), and summarized in the context of fully saturated flow in section S2 of the ESM.

Results

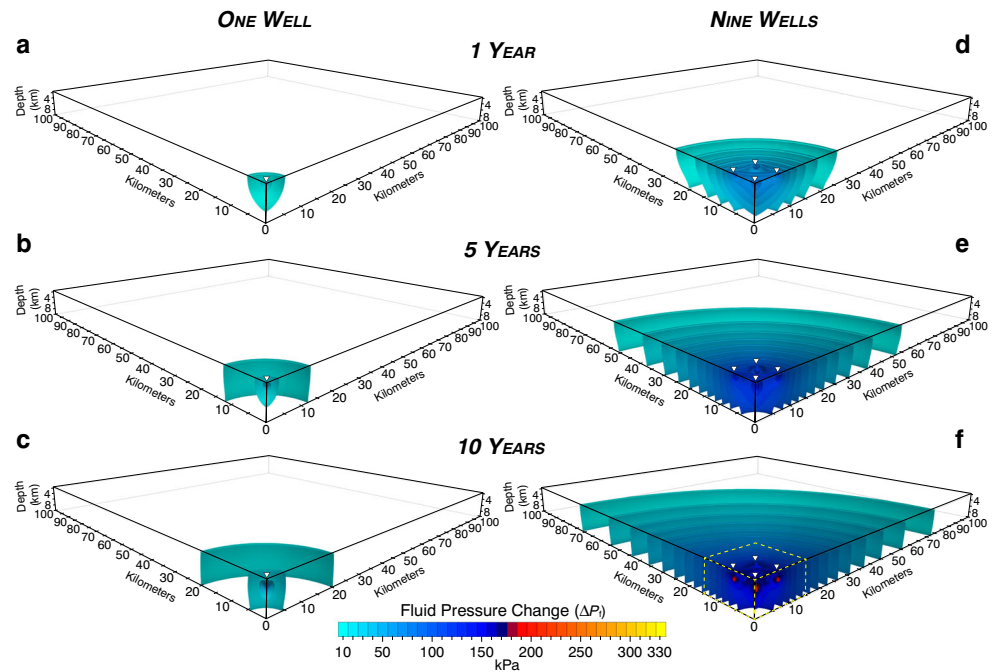
Model results are analyzed on the basis of fluid pressure above initial conditions (ΔP_i) and plotted as ΔP_i isosurface contours in 10-kPa intervals. Figure 3 presents simulation results during the injection phase after 1, 5, and 10 years for both the single well and nine-well scenarios. Figure 4 presents simulation results during the post-injection recovery phase after 1, 5, and 10 years for both the single well and nine-well scenarios. Figure 5 illustrates the hydrogeologic principle of superposition within a detailed section of the nine-well simulation results after 10 years of injection. Electronic Supplementary Information include simulation results for the three additional

Table 1 Model parameters

Medium	k -matrix (m^2)	k -fracture (m^2)	Porosity –	Density (kg m^{-3})	β (Pa^{-1})	k_T ($\text{W m}^{-1} ^\circ\text{C}^{-1}$)	c_p ($\text{J kg}^{-1} ^\circ\text{C}^{-1}$)	D ($\text{m}^2 \text{ s}^{-1}$)
Arbuckle	5×10^{-13}	–	0.1	2,500	1.7×10^{-10}	2.2	1,000	–
Basement	1×10^{-20}	$f(z)$	0.1	2,800	4.5×10^{-11}	2.2	1,000	–
Brine	–	–	–	1,123 ^a	–	–	–	1.14×10^{-9}
Water	–	–	–	–	–	–	–	2.30×10^{-9}

^a Reference density for EOS7, k -permeability, β -compressibility, k_T -thermal conductivity, c_p -heat capacity, D -diffusion coeff

Fig. 3 Simulated fluid pressure accumulation (ΔP_f) in 10-kPa contours for the one-well model (left column) and nine-well model (right column) after 1 year (**a, d**), 5 years (**b, e**), and 10 years (**c, f**) of oilfield wastewater disposal at $2,080 \text{ m}^3 \text{ day}^{-1} \text{ well}^{-1}$ ($13,000 \text{ bbl day}^{-1} \text{ well}^{-1}$). Injection occurs in the upper 200 m of the Arbuckle formation. Well positions are denoted with inverted triangles. All simulations invoke four-fold symmetry and only a one-quarter domain is simulated. The yellow-dashed box (**f**) is presented in Fig. 5 and animated in Movie S1 of the [ESM](#)



models with varying permeability structure (Figs. S2–S4 of the [ESM](#)) and Movie S1 of the [ESM](#) presents animated simulation results for the detailed section shown in Fig. 5.

Discussion

Fluid pressure changes as low as 10 kPa (0.1 bar) have been implicated in earthquake triggering (Reasenber and Simpson 1992). Results from the present study show that a single high-

rate injection well can drive a 10-kPa pressure front to lateral distances of 5, 12, and 20 km from the injection well after 1, 5, and 10 years, respectively (Fig. 3a–c). This result is congruent with many research studies that show injection-induced earthquakes generally occur within ~20 km of injection operations, e.g., Yeck et al. (2014). In contrast, the model scenario simulating the effects of nine high-rate injection wells drives the 10-kPa pressure front beyond 20, 50, and 70 km from the well cluster after 1, 5, and 10 years, respectively (Fig. 3d–f). The phenomenon in which multiple injection wells drives long-

Fig. 4 Isosurface contours of fluid pressure above initial conditions (ΔP_f) in 10-kPa contours for the single well model (left column) and nine-well model (right column) after 1 year (**a, d**), 5 years (**b, e**), and 10 years (**c, f**) of post-injection recovery. Well positions are denoted with inverted triangles. All simulations invoke four-fold symmetry and only a one-quarter domain is simulated.

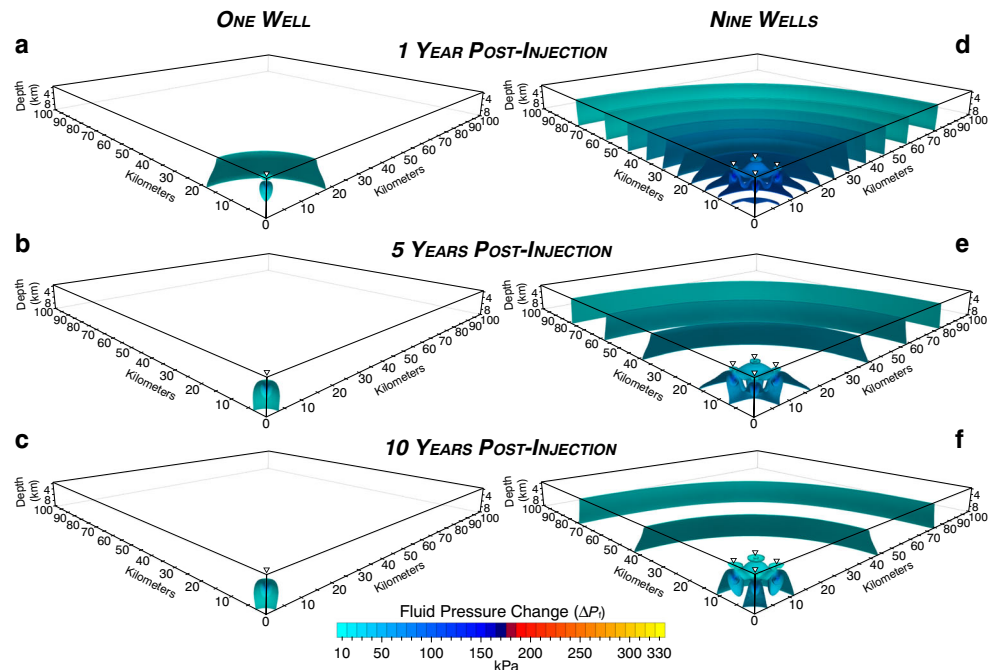
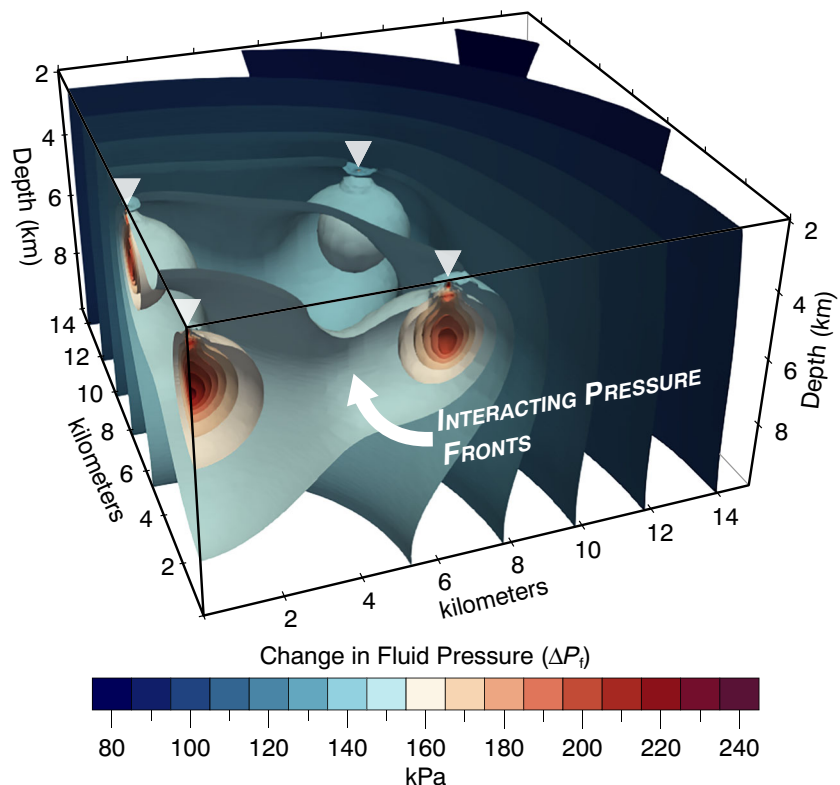


Fig. 5 Detailed section of callout in Fig. 3f showing the hydrogeological principle of superposition as interacting pressure fronts that locally increase the hydraulic gradient to drive long-range pressure accumulation. Isosurface contours illustrate fluid pressure above initial conditions (ΔP_f) in 10-kPa isosurface contours. Inverted triangles denote well locations. Movie S1 of the [ESM](#) presents an animation of pressure propagation within the section illustrated here. Note model invokes four-fold symmetry, so only a one-quarter domain is shown and the color ramp is restricted to the ΔP_f range for this section of the model.



range pressure transients is consistent across the complete set of basement permeability scenarios (Fig. 3, S2–S4 of the [ESM](#)), which suggests that the lateral extent of long-range pressure transients is generally insensitive to basement permeability. Nevertheless, these results show that basement permeability does influence the shape of the migrating pressure front. Within the highest permeability scenario (Fig. S2 of the [ESM](#)), fluid pressure tends to advance uniformly throughout the seismogenic zone. In contrast, the lower permeability scenarios (Fig. 3, S3–S4 of the [ESM](#)) show that pressure accumulation reaches greater lateral extent at shallow depths because the lower permeability structure inhibits pressure propagation at greater depth. This effect is increasingly pronounced for the sequentially decreasing permeability scenarios. The influence of basement permeability is most pronounced during post-injection pressure recovery, when the absence of continued loading causes the far-field pressure to front collapse around the injection well(s) (Fig. 4). Results from this study also show that lower permeability scenarios delay pressure recovery, thus maintaining elevated fluid pressure long after injection operations cease (Figs. S3–S4 of the [ESM](#)).

In comparing the lateral extent of pressure propagation between the single- and nine-well model scenarios, it is important to note that the nine-well model scenario injects $9\times$ more wastewater into the system than the single well scenario. This results in a proportionately greater dynamic load and reasonably explains why the nine-well scenario generates higher fluid pressure over longer distances. However, the

discrepancy in wastewater injection volume between each scenario does not explain *how* pressure transients from individual wells in the nine-well scenario contribute to the cumulative pressure front. For example, the fluid pressure generated from each well in the nine-well scenario (Fig. 3d–f) is identical to the pressure response radiating from the single-well scenario (Fig. 3a–c) because all wells operate at $2,080 \text{ m}^3 \text{ day}^{-1}$. If the pressure fronts from each well in the nine-well scenario propagate independent of one another, then the cumulative pressure front would simply translate the single-well pressure front to each well location in the nine-well scenario. This would put the 10-kPa isosurface contour approximately 25–30 km from the central well after 10 years because wells in the nine-well scenario are spaced 6 km apart. However, the pressure front radiating from the nine-well model is more than twice this distance, which suggests that the pressure fronts radiating from each individual well are interacting with one another in a manner that compounds individual pressure fronts into a larger cumulative effect. This phenomenon is present in previous modeling studies that show or mention coalescing pressure fronts (e.g., Keranen et al. 2014; Goebel et al. 2017), but the fundamental hydrogeological process responsible this phenomenon has not been clearly articulated in the literature.

In groundwater hydraulics, the compounding nature of hydrogeological perturbations is based on the *principle of superposition*, which states that “...the solution to a problem involving multiple inputs is equal to the sum of the solutions

to a set of simpler individual problems that form the composite problem” (Reilly et al. 1984). This means that the groundwater response to multiple pumping wells is the sum of the groundwater response for each individual well. As a consequence, the cumulative effect of multiple pumping wells is additive. The principle of superposition is traditionally taught in undergraduate hydrogeology courses in the context of groundwater withdrawals, e.g., capture zone analysis, image well analysis, time-drawdown pump test analysis (Fitts 2012). In this context, superposition explains why drawdown increases faster when there is an intersection between cones of depression from nearby pumping wells. In the context of oilfield wastewater disposal, this concept is simply inverted so that pressure accumulates faster when pressure fronts from nearby injection wells intersect one another. The additive nature of superposition means that the hydraulic gradient locally increases when pressure fronts intersect and merge. This increases the energy potential within the groundwater system, which drives pressure transients longer distances than estimates predicted by either single-well models or triggering front calculations based on classical root-time scaling laws for pressure diffusion from individual wells.

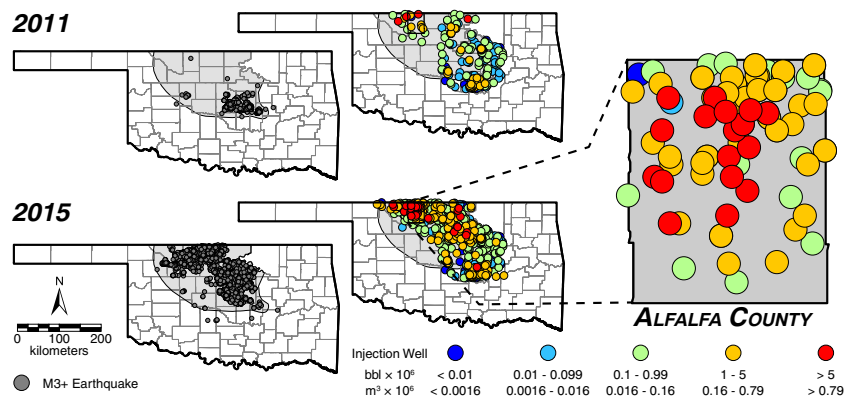
To illustrate how the principle of superposition drives long-range pressure accumulation, Fig. 5 presents a detailed section of the nine-well model after 10 years of injection and Movie S1 of the [ESM](#) shows its temporal progression in 6-month intervals from 3 to 10 years. These graphics show that pressure fronts nucleate at injection wells, radiate laterally, and then merge to produce a volume of overpressure that encompasses a greater areal extent than is possible for individual wells operating in isolation. As this process continues, the cumulative result is long-range pressure diffusion that continues so long as the dynamic load is maintained from the injection wells. To further explore the nature of superposition, the nine-well model was repeated so that each well injects $231 \text{ m}^3 \text{ day}^{-1}$ ($1,444 \text{ bbl day}^{-1}$), which results in a total injection volume of $2,080 \text{ m}^3 \text{ day}^{-1}$ ($13,000 \text{ bbl day}^{-1}$). This effectively distributes the total injection volume from the single-well model evenly across the nine-well model. Results for this simulation (Fig. S5 of the [ESM](#)) show that the 10 kPa pressure front reaches the

same lateral extent ($\sim 20 \text{ km}$) as the single well model (Fig. 3) after 10 years of injection; however, this result also finds that fluid pressure recovers much faster when the injection volume is distributed over a larger area. In the context of injection-induced earthquake hazard mitigation, this result demonstrates that total volume of wastewater injected is a more fundamental control on long-range fluid pressure transients than the total number of injection wells; however, it is also clear that distributing a given wastewater volume over multiple wells results in faster post-injection fluid pressure recovery.

Because this modeling study is based on the injection rates and geology from the Anadarko Shelf near the Oklahoma-Kansas border, the principle of superposition reasonably explains the observations of long-range pressure transients and earthquake triggering reported in south-central Kansas by Peterie et al. (2018). This inference is further supported by the spatial distribution of wastewater injection wells in Alfalfa County, Oklahoma, which experienced a dramatic increase in the number of wastewater disposal wells and M3+ earthquakes between 2011 and 2015 (Fig. 6). In 2011, the spatial distribution of wastewater injection wells was relatively sparse and there was only one high-rate injector ($>2,000 \text{ m}^3 \text{ day}^{-1}$). By 2015, the mean nearest-neighbor distance between injection wells was less than 1.5 km, and there were 17 high-rate injection wells (Fig. 6, red circles). The simulations presented here suggest that pressure fronts radiating from numerous, closely spaced high-rate injection wells at the Oklahoma-Kansas border are merging to drive long-range pressure accumulation into south-central Kansas.

In the post-injection recovery phase, the simulations developed here also show that fluid pressure continues increasing at systematically greater depths as high-density wastewater sinks and displaces lower density host rock fluids (Fig. 4d–f). This phenomenon has been implicated in systematically decreasing earthquake hypocenter depths in northern Oklahoma and southern Kansas (Pollyea et al. 2019). The simulation results presented here further indicate that the principle of superposition explains how these residual pressure fronts merge to produce a region of elevated fluid pressure that systematically deepens even after injection operations cease (Fig. 4d–f).

Fig. 6 North-central Oklahoma experienced dramatic growth in the number of oilfield wastewater disposal wells and M3+ earthquakes from 2011 to 2015. In Alfalfa County, the mean nearest-neighbor well spacing was less than 1.5 km in 2015 (Pollyea et al. 2018a). Earthquake data from USGS ComCat database (USGS 2019) and wastewater disposal data from Oklahoma Corporation Commission (OCC 2018)



Whereas previous studies allude to “merging” or “coalescing” pressure fronts during oilfield wastewater disposal (e.g., Goebel et al. 2017), this study shows that the hydrogeological principle of superposition is the mechanistic process responsible for this phenomenon. Moreover, this study shows that the principle of superposition reasonably explains *how* a well field comprising just nine closely spaced, high-rate injection wells can drive long-range fluid pressure transients to 70+ km from the well cluster. And while this may seem intuitive to the trained hydrogeologist, there has yet to be a thorough examination of the hydrogeological processes governing long-range pressure transients. As a consequence, statistical analyses of long-range earthquake triggering (Pollyea et al. 2018a) are met with skepticism (Wilmoth 2018) and observations of long-range fluid pressure do not have a defensible mechanistic explanation (Peterie et al. 2018). Without a mechanistic explanation affected communities cannot resolve the question of culpability when injection-induced earthquakes cause damage. Specifically, who is responsible if one wastewater injection well pumps for years without seismicity, and then a second (or third, fourth, ..., *n*th) comes online and earthquakes begin? Of course, the first operator will argue that years passed without incident, so responsibility must lie with the other operators. Yet the principle of superposition implies that the question of culpability is much more complex because the cumulative effects of multiple injection wells are additive.

Conclusions

This study demonstrates that the hydrogeologic principle of superposition is the mechanistic process governing long-range fluid pressure transients during oilfield wastewater disposal. The principle of superposition states that the cumulative effects of multiple pumping wells are additive. This phenomenon is demonstrated by interrogating results from a hypothetical numerical groundwater model with geological, thermal, and fluid properties typical of the Anadarko Shelf region in north-central Oklahoma and south-central Kansas. The models are used to compare fluid pressure transients radiating from an isolated wastewater injection well and a well-field comprising nine closely spaced injection wells. Results from this study are summarized in the following:

1. When wastewater injection wells are closely spaced, their pressure fronts interact and merge to locally increase the hydraulic gradient and drive long-range fluid pressure transients, i.e., the principle of superposition is the mechanistic explanation for long-range fluid pressure transients during regionally expansive oilfield wastewater disposal operations.
2. The cumulative effects of just nine injection wells can drive a 10-kPa pressure front to length scales exceeding

70 km from the well cluster. Because there are hundreds of wastewater disposal wells operating in Oklahoma and Kansas, the hydrogeologic principle of superposition reasonably explains (1) observations of long-range (90+ km) fluid pressure accumulation reported by Peterie et al. (2018) and (2) regional-scale (100+ km) joint spatial correlation between wastewater injection volume and earthquake occurrence reported by Pollyea et al. (2018a).

3. Long-range fluid pressure transients are governed by cumulative injection volume, rather than the number of injection wells within a given disposal reservoir; however, post-injection pressure recovery occurs faster when wastewater volume is distributed across multiple injection wells. Thus, more low-rate injection wells are likely better practice than individual high-rate injection wells for the same cumulative injection volume.
4. Long-range fluid pressure accumulation from multiple injection wells is generally insensitive to bulk permeability structure of the seismogenic zone.

In closing, the hypothetical models developed for this study comprise idealized geology that neglects detailed fault structures and hydro-mechanical couplings that are known to influence earthquake triggering processes. Nevertheless, this study does account for several hydrogeological phenomenon that are now known to be critically important to fluid pressure accumulation and recovery, specifically thermal effects on fluid flow and variable fluid composition between wastewater and host rock (Pollyea et al. 2019). As a result, this modeling study provides the hydrogeological basis to apply the principle of superposition as a framework to understand and deconvolve complex interactions between pressure transients when numerous wastewater injection wells operate in close spatial proximity. The application of these methods to real world sites requires substantial advances in (1) the ability to characterize complex geologic features and their hydraulic properties within the seismogenic zone, (2) availability and access to fluid property datasets within the seismogenic zone, and (3) efficient numerical simulation frameworks for modeling fully coupled thermal, hydraulic, chemical, and mechanical processes. The author hopes the discussion presented in this manuscript yields additional motivation to pursue these objectives.

Acknowledgements The author extends sincerest gratitude to Dr. Martin C. Chapman for insightful discussions about injection-induced seismicity. Computational resources were provided by Advanced Research Computing at Virginia Tech. The author also thanks Dr. Stuart Gilfillan and one anonymous reviewer for their thoughtful reviews of this manuscript. This study is based upon work supported by the US Geological Survey under Grant No. G19AP00011. The views and conclusions contained in this document are those of the authors and should not be interpreted as representing the opinions or policies of the US Geological Survey. Mention of trade names or commercial products does not constitute their endorsement by the US Geological Survey. The author declares no conflict of interest.

References

- Blondes M, Gans KD, Engle MA, Kharaka YK, Reidey ME, Saraswathula Y, Thordsen JJ, Rowan EL, Morrissey EA (2017) USGS National Produced Waters Geochemical Database v2.3. <https://energy.usgs.gov/Portals/0/Rooms/producedwaters/tabular/USGSPWDBv2.3c.csv>. Accessed 13 June 2018
- Brown MR, Ge S, Sheehan AF, Nakai JS (2017) Evaluating the effectiveness of induced seismicity mitigation: numerical modeling of wastewater injection near Greeley, Colorado. *J Geophys Res Solid Earth* 122(8):6569–6582
- Cranganu C, Lee Y, Deming D (1998) Heat flow in Oklahoma and the south-central United States. *J Geophys Res Solid Earth* 103(B11):27107–27121
- Ellsworth WL (2013) Injection-induced earthquakes. *Science* 341(6142). <https://doi.org/10.1126/science.1225942>
- Fitts CR (2012) *Groundwater science*, 2nd edn. Elsevier, Amsterdam
- Goebel TH, Brodsky EE (2018) The spatial footprint of injection wells in a global compilation of induced earthquake sequences. *Science* 361(6405):899–904
- Goebel THW, Weingarten M, Chen X, Haffener J, Brodsky EE (2017) The 2016 Mw5.1 Fairview, Oklahoma earthquakes: evidence for long-range poroelastic triggering at >40 km from fluid disposal wells. *Earth Planet Sci Lett* 472:50–61
- Hearn EH, Koltermann C, Rubinstein JR (2018) Numerical models of pore pressure and stress changes along basement faults due to wastewater injection: applications to the 2014 Milan, Kansas earthquake. *Geochem Geophys Geosyst*. <https://doi.org/10.1002/2017GC007194>
- Hubbert MK, Willis DG (1957) *Mechanics of hydraulic fracturing*, 210. Petroleum Transactions, AIME, New York
- Johnson KS (1991) Geologic overview and economic importance of late Cambrian and Ordovician age rocks in Oklahoma. In: Johnson KS (ed) *Late Cambrian-Ordovician geology of the southern midcontinent*. 1989 symposium, Oklahoma Geol Surv Circ 92, pp 3–14
- Jung Y, Pau GSH, Finsterle S, Pollyea RM (2017) TOUGH3: a new efficient version of the TOUGH suite of multiphase flow and transport simulators. *Comput Geosci* 108:2–7. <https://doi.org/10.1016/j.cageo.2016.09.009>
- Jung Y, Pau G, Finsterle S, Doughty C (2018) TOUGH3 user's guide: version 1.0. Tech. Rep. LBNL-2001093, Lawrence Berkeley National Laboratory. http://tough.lbl.gov/assets/files/Tough3/TOUGH3_Users_Guide_v2.pdf. Accessed November 2019
- Keranen KM, Weingarten M, Abers GA, Bekins BA, Ge S (2014) Sharp increase in central Oklahoma seismicity since 2008 induced by massive wastewater injection. *Science* 345(6195):448–451
- Keranen KM, Savage HM, Abers GA, Cochran ES (2013) Potentially induced earthquakes in Oklahoma, USA: links between wastewater injection and the 2011 Mw 5.7 earthquake sequence. *Geology* 41(6):699–702
- Langenbruch C, Weingarten M, Zoback MD (2018) Physics-based forecasting of man-made earthquake hazards in Oklahoma and Kansas. *Nat Commun* 9(1):3946
- Manning CE, Ingebritsen SE (1999) Permeability of the continental crust: implications of geothermal data and metamorphic systems. *Rev Geophys* 37(1):127–150
- Mao S, Duan Z (2008) The PVT properties of aqueous chloride fluids up to high temperatures and pressures. *J Chem Thermodyn* 40:1046–1063
- National Research Council (NRC) (2013) *Induced seismicity potential in energy technologies*. National Academies Press, Washington, DC. <https://doi.org/10.17226/13355>
- OCC (2018) Oil and gas data files, Oklahoma Corporation Commission (OCC). <http://www.occeweb.com/og/ogdatafiles2.htm>. Accessed 23 December 2018
- Ogwari PO, DeShon HR, Hornbach MJ (2018) The Dallas-Fort Worth airport earthquake sequence: seismicity beyond injection period. *J Geophys Res Solid Earth* 123(1):553–563
- Peterie SL, Miller RD, Intfen JW, Gonzales JB (2018) Earthquakes in Kansas induced by extremely far-field pressure diffusion. *Geophys Res Lett* 45(3):1395–1401
- Pollyea RM, Mohammadi N, Taylor JE, Chapman MC (2018a) Geospatial analysis of Oklahoma (USA) earthquakes (2011–2016): quantifying the limits of regional-scale earthquake mitigation measures. *Geology* 46(3):715–718. <https://doi.org/10.1130/G39945.1>
- Pollyea RM, Jayne RS, Wu H (2018b) The effects of fluid density variations during oilfield wastewater disposal. In: Oldenburg, C (ed) *Proceedings of the TOUGH Symposium 2018*. Berkeley, CA, October 8–10, 2018
- Pollyea RM, Chapman MC, Jayne RS, Wu H (2019) High density oilfield wastewater disposal causes deeper, stronger, and more persistent earthquakes. *Nat Commun* 10. <https://doi.org/10.1038/s41467-019-11029-8>
- Raleigh CB, Healy JH, Bredehoeft JD (1976) An experiment in earthquake control at Rangely, Colorado. *Science* 191(4233):1230–1237
- Reasenber PA, Simpson RW (1992) Response of regional seismicity to the static stress change produced by the Loma Prieta earthquake. *Science* 255(5052):1687–1690
- Reilly TE, Franke OL, Bennett GD (1984) The principle of superposition and its application in groundwater hydraulics. US Geol Surv Open File Rep 84-459. <https://doi.org/10.3133/ofr84459> and <https://pubs.usgs.gov/of/1984/0459/report.pdf>. Accessed December 2018
- Schoenball M, Walsh FR, Weingarten M, Ellsworth WL (2018) How faults wake up: the Guthrie-Langston, Oklahoma earthquakes. *Lead Edge* 37(2):100–106
- Shapiro SA, Krüger OS, Dinske C, Langenbruch C (2011) Magnitudes of induced earthquakes and geometric scales of fluid-stimulated rock volumes. *Geophysics* 76(6):WC55–WC63
- US Geological Survey (USGS) (2019) ANSS comprehensive earthquake catalog (ComCat). <https://earthquake.usgs.gov/earthquakes/search/>. Accessed March 2019
- Walsh FR, Zoback MD (2015) Oklahoma's recent earthquakes and salt-water disposal. *Sci Adv* 1(5). <https://doi.org/10.1126/sciadv.1500195>
- Weingarten M, Ge S, Godt JW, Bekins BA, Rubinstein JL (2015) High-rate injection is associated with the increase in US mid-continent seismicity. *Science* 348(6241):1336–1340
- Wilmoth A (2018) Oklahoma researcher dismisses Virginia Tech study of local earthquakes. *The Oklahoman*, Oklahoma City, OK, 11 January 2018. <https://newsok.com/article/5579064/oklahoma-researcher-dismisses-virginia-tech-study-of-local-earthquakes>. Accessed 12 January 2018
- Yeck WL, Block LV, Wood CK, King VM (2014) Maximum magnitude estimations of induced earthquakes at Paradox Valley, Colorado, from cumulative injection volume and geometry of seismicity clusters. *Geophys J Int* 200(1):322–336
- Zoback MD, Hickman S (1982) In situ study of the physical mechanisms controlling induced seismicity at Monticello reservoir, South Carolina. *J Geophys Res Solid Earth* 87(B8):6959–6974